Electronic Supplementary Information (ESI) for:

Unravelling the oxygen exchange mechanism on $La_2Ce_2O_7$

Yizhou Shen, Vincent Thoréton, Reidar Haugsrud

Department of Chemistry, Centre for Materials Science and Nanotechnology, University of Oslo, Gaustadalléen 21, NO-0349 Oslo, Norway

1 Gas phase analysis

The Pulse Isotope Exchange (PIE) method relies on a set of prerequisites to yield adequate data. These include: 1) all exchange species are equivalent, 2) constant volume of the gas in the PIE bed reactor, 3) both the gas and solid phase are homogeneous, i.e., fast diffusion occurs in both the gas and solid phases, 4) the number of adsorbed oxygen species on the surface, compared to the total oxygen involved in the exchange process in the system, can be neglected, and 5) ideal plug flow behavior prevails during the oxygen isotope exchange measurement [1]. Under conditions where these requirements are met, the change in the fraction of ^{18}O in the gas phase, f_g^{18}, can be derived based on the reversible oxygen exchange reaction (Eq. 1 in the main text) by solving the first-order linear differential equation [2]:

$$n\frac{\partial f_g^{18}}{\partial t} = -R_0 S(f_g^{18} - f_b^{18}) \tag{1}$$

where n is the number of moles of oxygen atoms in the gas phase, S represents the total surface area of the oxide powders, f_b^{18} denotes the ^{18}O isotope fraction in the oxide bulk and R_0 is the overall oxygen surface exchange rate. The fraction of the ^{18}O isotope in the gas phase is determined from the molar fractions of $^{16}O^{18}O$ (f_g^{34}) and $^{18}O_2$ (f_g^{36}), respectively as measured by means of gas-phase mass spectrometry:

$$f_g^{18} = f_g^{36} + \frac{1}{2}f_g^{34} \tag{2}$$

Furthermore, when ^{18}O in the oxide is negligible, an explicit equation for the surface exchange rate can be obtained:

$$R_0 = -\frac{n}{\tau S}\ln\frac{f_{g,o}^{18}}{f_{g,i}^{18}} \tag{3}$$

where $f_{g,i}^{18}$ and $f_{g,o}^{18}$ represent the ^{18}O isotope fractions in the gas phase at the inlet and outlet of the reactor, respectively. τ represents the residence time of the reactor bed, describing the average reaction time between the oxygen molecules in the pulse and the powder:

$$\tau = \frac{V\varepsilon}{F} \tag{4}$$

V denotes the volume of the packed-bed reactor, ε is the bed void fraction and F represents the volumetric flow rate of the carrier gas at chosen temperature. The oxygen surface exchange coefficient k_s and the exchange rate is further related by [3]:

$$k_s = \frac{R_0}{C_O} \tag{5}$$

where c_O is the concentration of lattice oxygen. R_0 is a lumped parameter including the rates for a series of elementary surface processes at equilibrium, often predominated by the slowest process, i.e., the rate-determining step (RDS). Boukamp *et al.* [4] proposed a serial two-step model where the overall oxygen exchange is split into two sub-reactions; the dissociative adsorption of oxygen molecules with reaction rate R_{dis} and the incorporation of oxygen adatoms into the lattice with a reaction rate R_{inc}. To better describe the relations of the two rate constants with respect to the overall exchange rate R_0 and compare them with other proposed models and mechanisms, two stochastic parameters, p_1 and p_2, were introduced by Den Otter *et al.* [5]. These parameters signify the independent probabilities for each atom in the diatomic oxygen molecule to incorporate into the oxide lattice. Den Otter et al., defined expectation fractions (α_1 and α_2) to find ^{18}O-labeled oxygen in the O_2 molecule after an isotopic exchange at the outlet of the reactor are formulated as follows:

$$\begin{cases} \alpha_1 = p_1 f_b^{18} + (1 - p_1) f_g^{18} \\ \alpha_2 = p_2 f_b^{18} + (1 - p_2) f_g^{18} \end{cases} \tag{6}$$

Differential equations for f_g^{36}, f_g^{34} and f_g^{32} can be written as:

$$\begin{cases} \dfrac{n}{SR_{dis}}\dfrac{df_g^{36}}{dt} = -f_g^{36} + \alpha_1\alpha_2 \\ \dfrac{n}{SR_{dis}}\dfrac{df_g^{34}}{dt} = -f_g^{34} + \alpha_1(1-\alpha_2) + (1-\alpha_1)\alpha_2 \\ \dfrac{n}{SR_{dis}}\dfrac{df_g^{32}}{dt} = -f_g^{32} + (1-\alpha_1)(1-\alpha_2) \end{cases} \tag{7}$$

Inserting (7) into (2) and assuming $f_b^{18} \approx 0$, the differential equation for f_g^{18} is derived as:

$$n\frac{\partial f_g^{18}}{\partial t} = -\frac{1}{2}S(p_1+p_2)R_{dis}f_g^{18} \tag{8}$$

Compared to (1), R_{dis} can be related to R_0 as follows:

$$R_0 = \frac{1}{2}(p_1+p_2)R_{dis} \tag{9}$$

If the two oxygen adatoms have an equal probability of being incorporated into the lattice,

$$p_1 = p_2 = p \tag{10}$$

under the steady state approximation where:

$$p = \frac{R_{inc}}{R_{dis}+R_{inc}} \tag{11}$$

R_0 can be further related to R_{dis} and R_{inc} as:

$$R_0 = pR_{dis} \tag{12}$$

$$R_0 = \frac{R_{dis}R_{inc}}{R_{dis}+R_{inc}} \tag{13}$$

$$\frac{1}{R_0} = \frac{1}{R_{dis}} + \frac{1}{R_{inc}} \tag{14}$$

$$\begin{cases} R_{dis} = \dfrac{R_0}{p} \\ R_{inc} = \dfrac{R_0}{1-p} \end{cases} \tag{15}$$

In this scenario, the incorporation occurs only after the dissociative adsorption, corresponding to a *serial* process as indicated by Eqs. 4.b and 5.b in the main text. The fraction of $^{18}O_2$ at the outlet of the reactor is further derived by inserting (3) and (10) into (7):

$$\frac{np\,df_g^{36}}{SR_0\,dt} = -f_g^{36} + [(1-p)f_g^{18}]^2 \tag{16}$$

$$f_{g,o}^{36} = \left(\frac{1-p}{(1-2p)^{\frac{1}{2}}} f_{g,i}^{18}\right)^2 e^{-\frac{2R_0 S\tau}{n}} + \left[f_{g,i}^{36} - \left(\frac{1-p}{(1-2p)^{\frac{1}{2}}} f_{g,i}^{18}\right)^2\right] e^{-\frac{R_0 S\tau}{np}} \tag{17}$$

Alternatively, one of the two oxygen atoms in the oxygen molecule can be immediately incorporated into the lattice as part of the dissociative adsorption of the oxygen molecule, resulting in a *parallel-like* scheme for the overall oxygen exchange, as described by Eqs. 4.a and 5.a in the main text.

In this case, the relation between R_0, R_{dis} and R_{inc} can be derived according to Eq. 9:

$$R_0 = \frac{1}{2}(1+p')R_{dis} \tag{18}$$

with

$$p' = \frac{R_{inc}}{\frac{1}{2}R_{dis} + R_{inc}} \tag{19}$$

$$\begin{cases} R_{dis} = \dfrac{2R_0}{1+p'} \\ R_{inc} = \dfrac{p'R_0}{1-p'^2} \end{cases} \tag{20}$$

The fraction of $^{18}O_2$ at the outlet of the reactor is given as:

$$\frac{n(1+p')df_g^{36}}{2SR_0\quad dt} = -f_g^{36} \tag{21}$$

$$f_{g,o}^{36} = f_{g,i}^{36} e^{-\frac{2R_0 S\tau}{n(1+p')}} \tag{22}$$

For both the *serial* and *parallel* model, the fractions of the other isotopologues can be calculated as follows:

$$f_g^{34} = 2(f_g^{18} - f_g^{36}) \tag{23}$$

$$f_g^{32} = 1 - f_g^{36} - f_g^{34} \tag{24}$$

2 Relation to other models

In the isotopic exchange theory developed by Klier *et al.* [6] and Boreskov and Muzykantov [7], the exchange process is instead elucidated through three types of one-step exchange reactions. According to these theories, the O_2 molecule can exchange without involving lattice oxygen, i.e., only with oxygen atoms from the gas phase (termed homo exchange), at a rate R. Furthermore, it can exchange either one or both of its atoms with lattice oxygen (termed hetero exchange) at rates R' and R'', respectively.

$$O^{18}O^{18} + O^{16}O^{16} \leftrightarrow 2O^{18}O^{16} \Big\} \; R \tag{25}$$

$$\left.\begin{matrix} O^{18}O^{18} + O_s^{16} \leftrightarrow O^{18}O^{16} + O_s^{18} \\ O^{18}O^{16} + O_s^{16} \leftrightarrow O^{16}O^{16} + O_s^{18} \end{matrix}\right\} R' \tag{26}$$

$$\left.\begin{matrix} O^{18}O^{18} + 2O_s^{16} \leftrightarrow O^{16}O^{16} + 2O_s^{18} \\ O^{18}O^{16} + 2O_s^{16} \leftrightarrow O^{16}O^{16} + O_s^{18} + O_s^{16} \\ O^{18}O^{16} + 2O_s^{18} \leftrightarrow O^{18}O^{18} + O_s^{18} + O_s^{16} \end{matrix}\right\} R'' \tag{27}$$

here, the subscript s denotes the surface. These rates can be related to the dissociative adsorption rate R_{dis}, the overall exchange rate R_0 and the two stochastic parameters p_1 and p_2 by:

$$\begin{cases} R &= R_{dis}(1-p_1)(1-p_2) \\ R' &= R_{dis}[p_1(1-p_2) + p_2(1-p_1)] \\ R'' &= R_{dis}p_1p_2 \end{cases} \tag{28}$$

$$R_{dis} = R + R' + R'' \tag{29}$$

$$R_0 = \frac{1}{2}R' + R'' \tag{30}$$

The relation between the serial- and parallel-model to the three one-step mechanisms can be visualized in the contour plots [5] of the fractions of R, $R^{'}$ and $R^{''}$ in R_{dis}, where pure homo exchange R and hetero exchange $R^{'}$ and $R^{''}$ correspond to the points (0,0), (0,1) or (1,0) and (1,1) respectively. The serial-model corresponds to the diagonal line, and the parallel-model corresponds to the horizontal line at the top and the vertical line on the right side. Recognizing the symmetrical feature of the contour plot, all the mechanisms along with the fitted p_1 and p_2 values for LaC and 5PrLaC under both dry and wet conditions at 750 °C and $p_{O_2} = 0.02\ atm$ are plotted in ESI Figures 1–3.

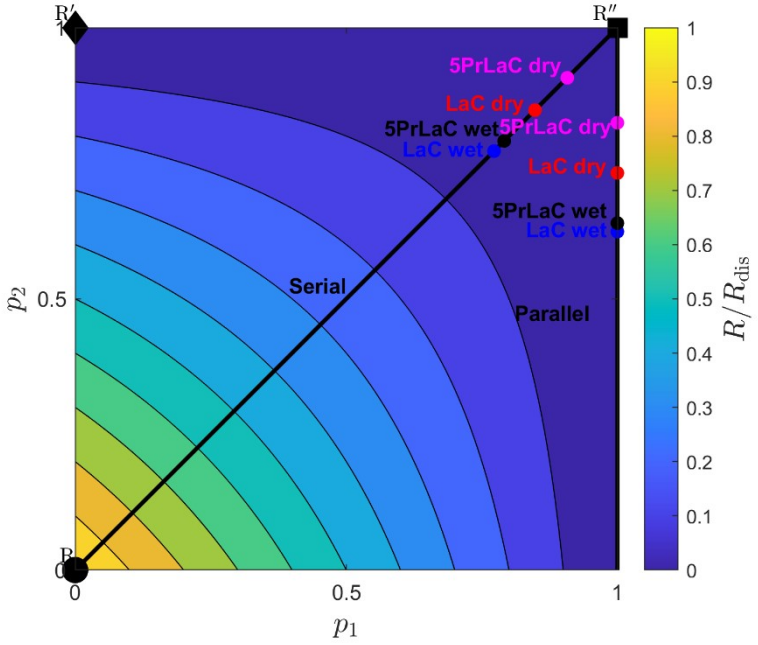

ESI Figure 1. *Contour plot of the ratio of the homo exchange rate to the dissociative adsorption rate.*

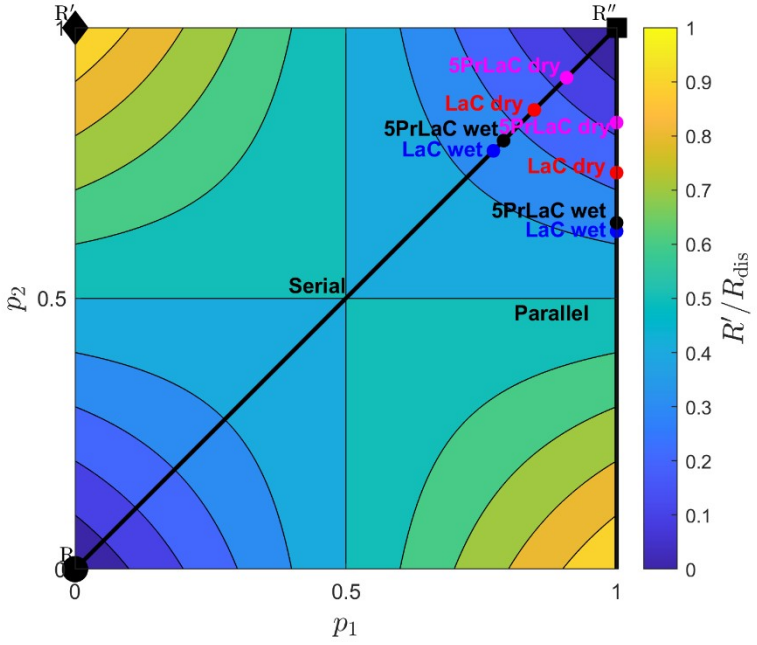

ESI Figure 2. *Contour plot of the ratio of the hetero exchange rate (one atom involved) to the dissociative adsorption rate.*

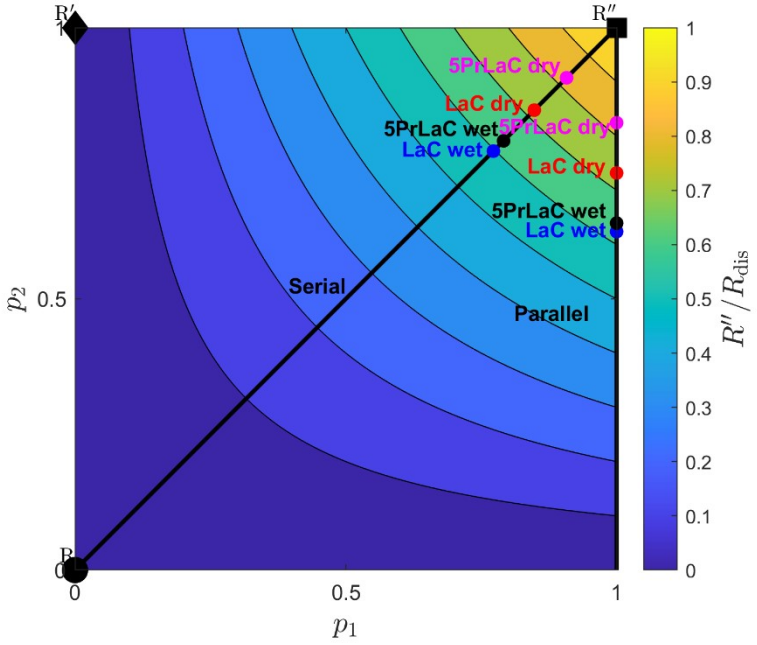

ESI Figure 3. *Contour plot of the ratio of the hetero exchange rate (two atoms involved) to the dissociative adsorption rate.*

According to Eq. 29, the lowest R/R_{dis} value corresponds to the highest $R^{'}/R_{dis}$ and $R^{''}/R_{dis}$ values in dry 5PrLaC, compared to wet 5PrLaC and dry/wet LaC. Since the parallel model

neglects the homo-exchange, R, which is not easy to recognize in the 2-D contour plot (ESI Figures 1–3), an increase in $R^{''}/R_{dis}$ results in a decrease in $R^{'}/R_{dis}$, and vice versa.

The relation between the rates in the *serial* and *parallel* models are further summarized in Eqs. 31 and 32, respectively.

$$\begin{cases} R = (1-p)^2 R_{dis} \\ R^{'} = 2p(1-p)R_{dis} \\ R^{''} = p^2 R_{dis} \end{cases} \quad (31)$$

$$\begin{cases} R = 0 \\ R^{'} = (1-p^{'}) R_{dis} \\ R^{''} = p^{'} R_{dis} \end{cases} \quad (32)$$

As shown in ESI Figure 2, the increase in the ratio of one-atom involved hetero exchange in 5PrLaC from dry to wet conditions is more pronounced in the *parallel* model compared to the *serial* model, better reflecting the higher f_g^{34} for 5PrLaC under wet conditions at 750 °C, as shown in Figure 2 of the main text.

3 XRD Results of the powder samples

As seen in ESI Figure 4, both materials are phase-pure. The introduction of Pr into $La_2Ce_2O_7$ results in a slight peak shift, as shown in the spectrum of 5Pr-$La_2Ce_2O_7$, indicating a minor increase in the lattice parameters. According to Vegard's law [8], the increase in lattice parameters reflects substitution of Ce^{4+}-ion (0.97 Å) with the larger Pr^{3+}-ion (1.126 Å) [9].

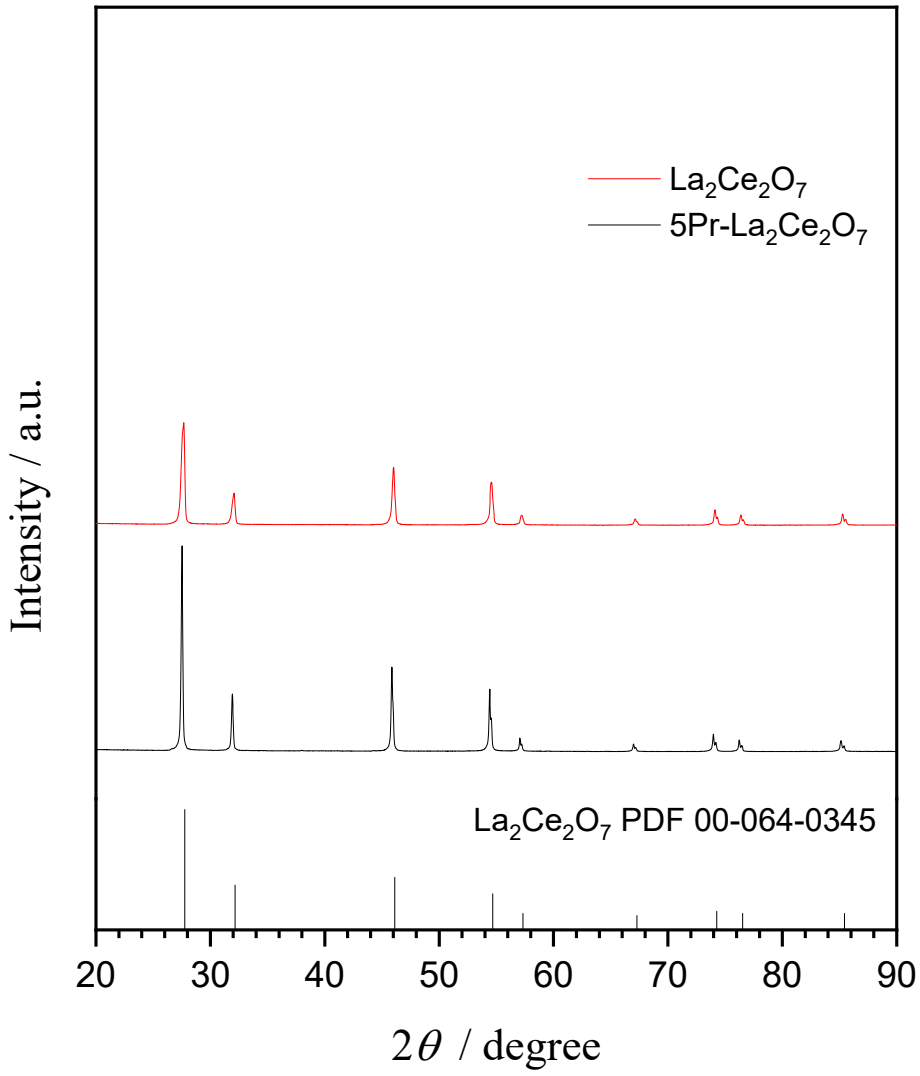

ESI Figure 4. *XRD patterns of $La_2Ce_2O_7$ and 5Pr-$La_2Ce_2O_7$.*

4 SEM Results of the powder samples

ESI Figure 5 presents scanning electron micrographs of the powder samples. The average grain size is approximately 50 µm, and the samples show high relative density with some (<5%) closed porosity.

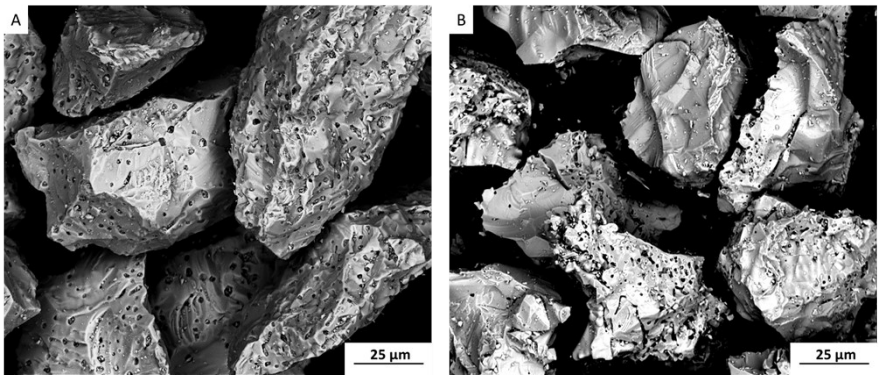

ESI Figure 5. *SEM images of A) $La_2Ce_2O_7$ powders and B) 5Pr-$La_2Ce_2O_7$ powders obtained from the back-scatter electron (BSE) detector.*

5 p_{O_2} dependences and activation energies of all deconvoluted R_{dis} and R_{inc}

In ESI Figures 6 and 7, R_{inc} obtained from the parallel-model (R_{inc}^{p} in the main text) is noticeably smaller than that from the serial-model (R_{inc}^{s} in the main text) within the same material. The differences in p_{O_2} dependences for R_{dis} and R_{inc} in LaC and 5PrLaC support the conclusion in the main text that the surface exchange mechanisms for these two materials are different, with the *serial* mechanism for LaC and the *parallel* mechanism for 5PrLaC, respectively.

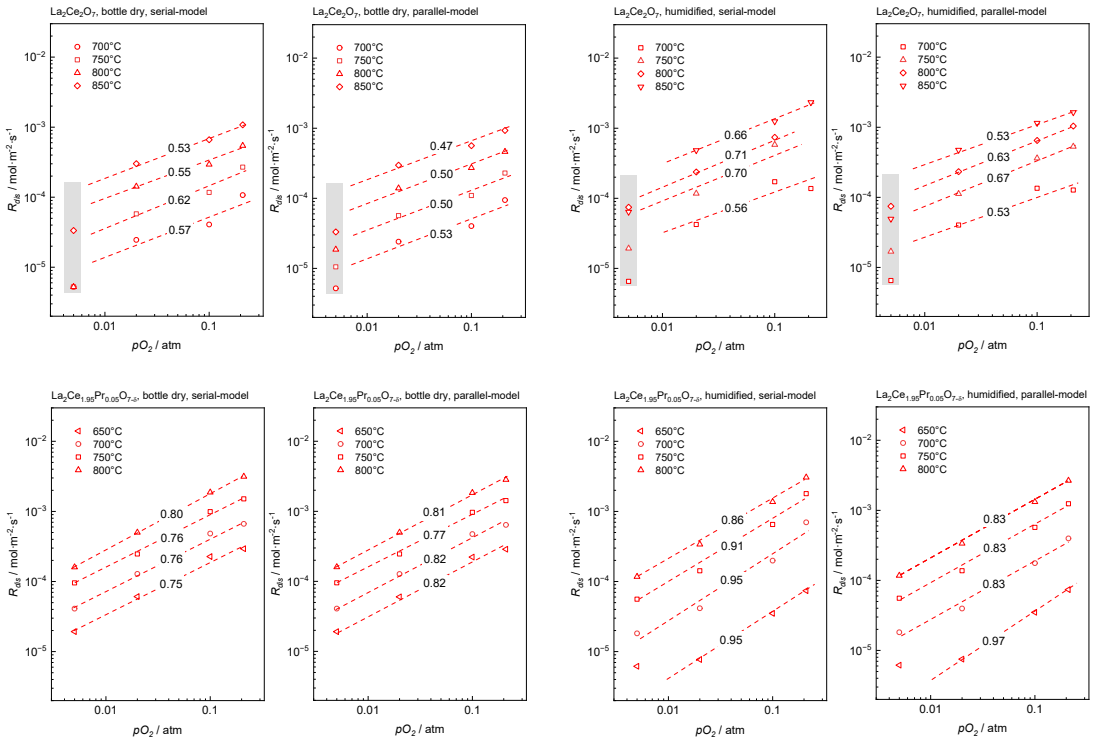

ESI Figure 6. *p_{O_2} dependences of all deconvoluted R_{dis} based on the two-step model.*

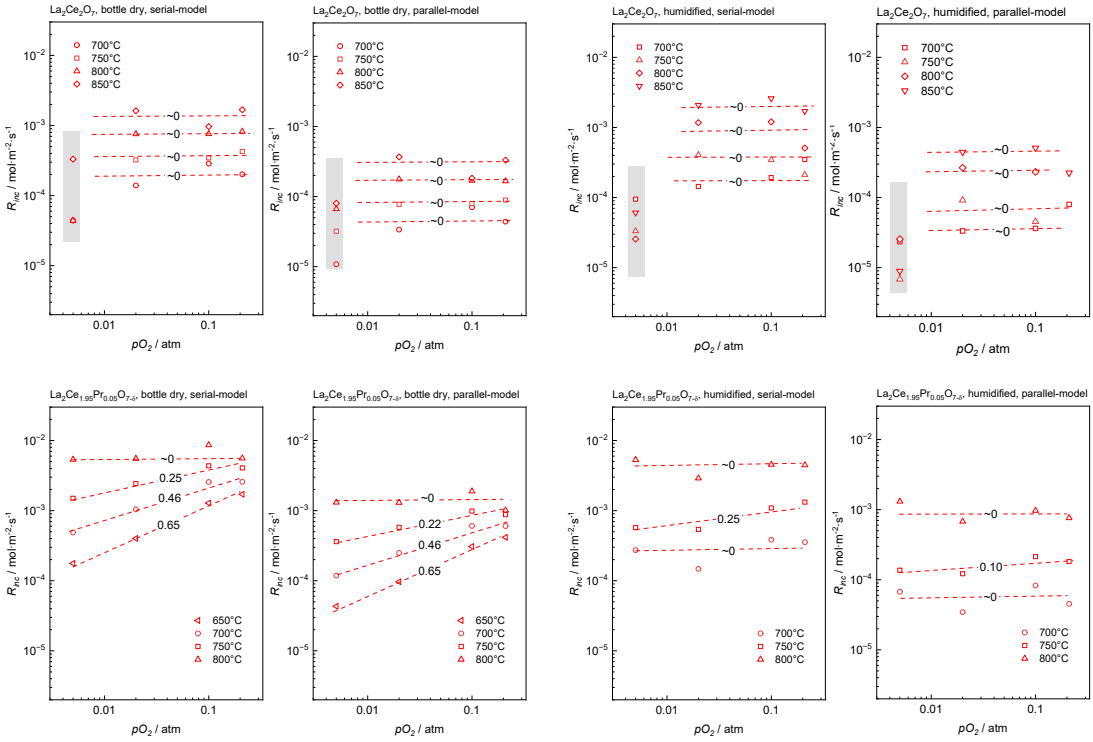

ESI Figure 7. *p_{O_2} dependences of all deconvoluted R_{inc} based on the two-step model.*

ESI Figure 8 presents the activation energies for all the equilibrium rates. However, some data points are missing due to insufficient data, which is particularly pronounced for LaC, especially under humidified conditions.

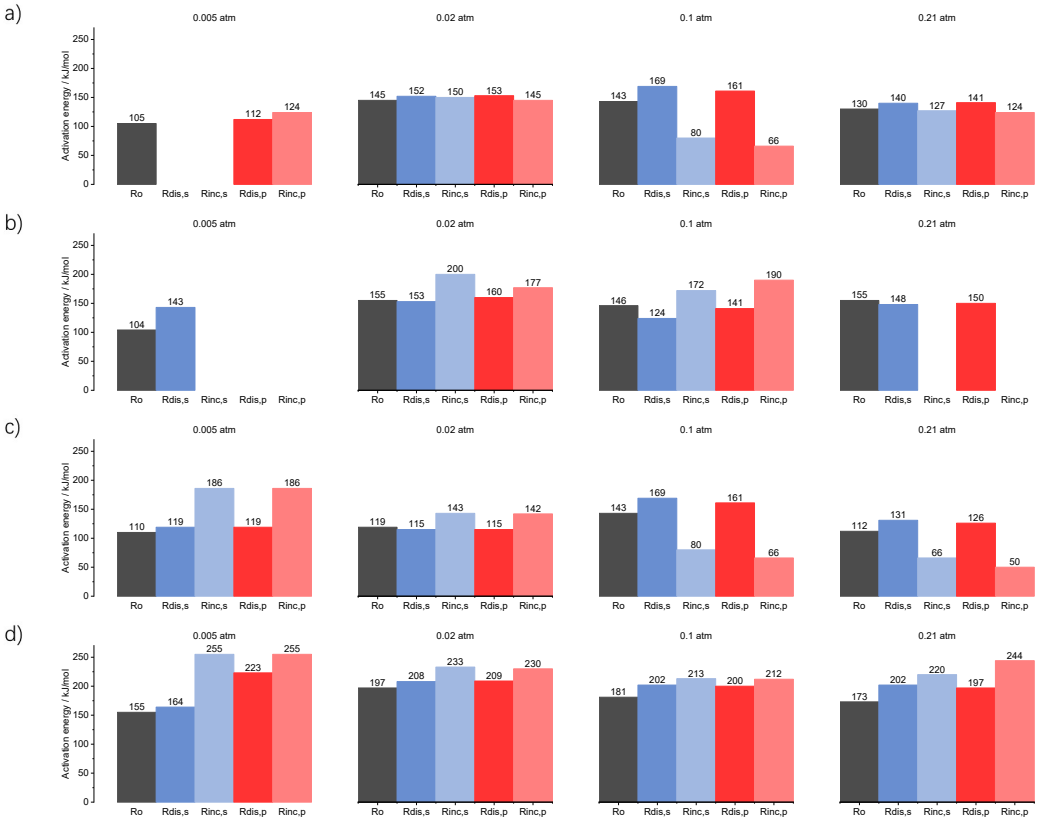

ESI Figure 8. *Activation energies for all the equilibrium rates: a) LaC bottle dry, b) LaC humidified, c) 5PrLaC bottle dry and d) 5PrLaC humidified.*

Reference

1 H. J. M. Bouwmeester, C. Song, J. Zhu, J. Yi, M. Van Sint Annaland and B. A. Boukamp, in *Physical Chemistry Chemical Physics*, 2009, vol. 11, pp. 9640–9643.

2 K. Klier and E. Kučera, *J. Phys. Chem. Solids*, 1966, **27**, 1087–1095.

3 C. Y. Yoo, B. A. Boukamp and H. J. M. Bouwmeester, *J. Solid State Electrochem.*, 2011, **15**, 231–236.

4 H. J. M. B. and A. J. B. B. A. Boukamp, in *Proceedings of the Second International Symposium on Ionic and Mixed Conducting Ceramics*, ed. W. L. W. and H. L. T. T. A. Ramanarayanan, The Electrochemical Society, 1994, p. 141.

5 M. W. Den Otter, B. A. Boukamp and H. J. M. Bouwmeester, *Solid State Ionics*, 2001, **139**, 89–94.

6 K. Klier, J. Novakova and P. Jiru, *J. Catal.*, 1963, **484**, 479–484.

7 G. K. Boreskov and V. S. Muzykantov, *Ann. N. Y. Acad. Sci.*, 1973, **213**, 137–170.

8 H. W. King and Y. Lo Vegard, *J. Mater. Sci.*, 1921, **1**, 79–90.

9 R. D. Shannon, *Acta Crystallogr. Sect. A*, 1976, **32**, 751–767.